International Journal of Biological Macromolecules 141 (2019) 197–206

Contents lists available at ScienceDirect

International Journal of Biological Macromolecules

journal homepage: http://www.elsevier.com/locate/ijbiomac

PVA/(ligno)nanocellulose biocomposite films. Effect of residual lignin content on structural, mechanical, barrier and antioxidant properties

Eduardo Espinosa [a,*], Isabel Bascón-Villegas [a], Antonio Rosal [d], Fernando Pérez-Rodríguez [b], Gary Chinga-Carrasco [c], Alejandro Rodríguez [a]

[a] Chemical Engineering Department, Faculty of Science, University of Córdoba, Córdoba 14014, Spain
[b] Department of Food Science and Technology, Faculty of Veterinary, University of Córdoba, 14014 Córdoba, Spain
[c] RISE PFI, Høgskoleringen 6b, 7491 Trondheim, Norway
[d] Molecular Biology and Biochemical Engineering Department, University Pablo de Olavide, Seville, Spain

ARTICLE INFO

Article history:
Received 22 July 2019
Received in revised form 29 August 2019
Accepted 30 August 2019
Available online 31 August 2019

Keywords:
Nanocellulose
Biocomposite films
Lignin effect

ABSTRACT

Nanocelluloses with and without residual lignin were isolated from wheat straw. In addition, the effect of TEMPO-mediated oxidation on the production of lignin-containing nanocellulose was studied. The different nanocelluloses were used as reinforcing agent in Poly(vinyl alcohol) films. The morphology, crystallinity, surface microstructure, barrier properties, light transmittance, mechanical and antioxidant properties were evaluated. The translucency of films was reduced by the addition of nanocellulose, however, the ability to block UV-light increased from 10% for PVA to >50% using lignin-containing nanocellulose, and 30% for lignin-free samples. The mechanical properties increased considerably, however, for loads higher than 5% a negative trend was observed presumptively due to a clustering of nanocellulose components in PVA matrix. The barrier properties of the films were improved with the use of nanocellulose, especially at small amounts (1–3%). The antioxidant capacity of films was increased up to 10% using lignin-containing nanocellulose compared to 4.7% using PVA.

1. Introduction

Nowadays, the petrochemical-based compounds such as polyvinylchloride (PVC), polyethylene terephthalate (PET), polypropylene (PP), polyethylene (PE), polystyrene (PS) and polyamide (PA) are the most used polymers for food packaging [1]. However, due to its poor degradability in nature, these materials are causing a serious environmental problem on a global scale. Its low cost, high availability, good mechanical properties and high gas barrier properties are not enough for an increasingly environmentally conscious society, which demands the use of more environmentally friendly processes and materials. Nevertheless, the use of biodegradable polymers in packaging are limited in their capacity to be utilized at commercial stage due to the weaknesses related to performance, such as poor moisture barrier and mechanical properties [2].

Polyvinyl alcohol (PVA) is a fully biodegradable, biocompatible, semi-crystalline, non-toxic, and water-soluble synthetic polymer obtained by hydrolysis of polyvinyl acetate [3]. The PVA properties, such as chemical resistance, optical and physical properties indicate a large technological potential. This polymer has potential ability to form hydrogen bonding with the hydrophilic surfaces of biomaterials to produce green composites [4]. Due to this capability, PVA is combined with other components to improve its performance and barrier properties such as silver nanoparticles [5], zinc oxide [6], titanium oxide [7], etc. However, these elements are inorganic-natured which presents limited processability, biocompatibility and biodegradability. The macroscopic reinforcing components usually cause defects, resulting in a smaller reinforcing effect of the composites [8], nevertheless, the use of nanomaterials allows a uniform dispersion of the material in a given matrix, improving the chemical compatibility between the components and changing the molecular mobility, the relaxation behaviour, and therefore, the thermal and mechanical properties of the material. These nanomaterials present a high specific surface area, providing a larger reaction surface with the matrix, and as a result, a better reinforcing effect.

One of the most promising reinforcement of biocomposites (i.e. composites containing at least one biobased component) is the cellulosic fibers due their renewability, sustainability and abundance and therefore their low-cost. The structure of cellulose can be deconstructed by means of intense mechanical treatment to achieve nanometric sized cellulosic fibers known as cellulose nanofibers (CNF). CNF is one of the nanomaterials that together with the cellulose nanocrystals (CNC) and bacterial cellulose (BC), that are commonly classified as nanocelluloses. CNF has been widely used as a reinforcing agent in polymer matrices to improve mechanical properties and resistance to gas passage [9,10].

* Corresponding author at: Chemical Engineering Department, University of Córdoba, Campus of Rabanales, Marie-Curie Building, Ctra. N-IV, km. 396, 14014 Córdoba, Spain.
E-mail address: eduardo.espinosa@uco.es (E. Espinosa).

https://doi.org/10.1016/j.ijbiomac.2019.08.262
0141-8130/

Different types of nanocellulose can be used as reinforcing agent, however CNF presents a higher reinforcement effect due to the large aspect ratio in comparison with CNC and their entanglements, which assists in fiber-matrix and fiber-fiber load transfer, also facilitates the early occurrence of the strain hardening of polymer composites [11]. PVA has been used in combination with nanocellulose for many applications such as membranes for gas separation [12,13], xerogels [14], electronics composites [15], as well as composites for food packaging application [16,17]. Nanocellulose has great potential for use as a reinforcement in food packaging due to its excellent properties: high elastic modulus (140–150 GPa), low density, low thermal expansion coefficient in the axial direction, high specific surface areas and chemical reactivity, as well as its abundance and biodegradability [18–20].

Nanocellulose can be obtained from any source of lignocellulosic raw material, including agricultural waste. In recent years many agricultural residues have been studied for this purpose, such as cereal straws [21], banana plant [22], cotton linter [23], olive tree pruning [24], etc. This allows the integral use of natural resources favoring the circular economy and bioeconomy.

Many of the studies related to the production of nanocellulose have been focused on bleached chemical pulps, however, nanocellulose from unbleached kraft pulps have also been reported to provide good properties for barriers for packaging applications [25]. Nanocellulose from unbleached pulps contains residual lignin, heteropolysaccharides and extractives which can enable production at higher yields and lower cost [26]. Residual lignin content in nanocellulose presents several advantages such as an improved compatibility [27], higher fineness due to the radical scavenging property of lignin [28], less hydrophilicity [29], showing a better dispersion and improved reinforcement efficiency. Spence et al. [30,31] reported that the energy and chemical requirements in the production of nanocellulose with residual lignin showed promises results for packaging applications. In addition, lignin-containing nanocellulose may be of particular interests in sectors where lignin as a component may provide benefits such as biomedicine [32,33], thermoelectric components [34], carbon fibers [35] and batteries [36].

This study explores the use of lignin-containing nanocellulose compared to lignin-free nanocellulose on the final properties of biocomposite films, as well as the effect of TEMPO-mediated oxidation as pretreatment on the production of lignin-containing nanocellulose and its properties compared to mechanical pretreatment. For that, nanocellulose with and without residual lignin content were isolated from wheat straw via soda pulping process. Biocomposites films were prepared by mixing nanocellulose and PVA in distilled water with various content ratios and subsequently cast in petri dishes. The chemical structure (FTIR), crystallinity (XRD), optical properties, microstructure (SEM), antioxidant activity (ABTS assay), barrier gas properties (WVP and OTR) and mechanical properties of the films were studied.

2. Experimental

2.1. Materials

Wheat straws were provided by Ecopapel S.L. from cooperatives of Écija, Seville, Spain. Polyvinyl alcohol (M.W.: 146,000–186,000; and degree of hydrolysis +99%) was provided by Sigma Aldrich (Madrid, Spain). Other reagents used were: sodium chlorite (Honeywell), sodium hydroxide (Panreac), sodium bromide (Honeywell), 2,2,6,6-Tetramethyl-piperidin-1-oxyle TEMPO (Sigma Aldrich), sodium hypochlorite (Honeywell), Poly-Dadmac (BTG) and Pes-Na (BTG). All chemical reagents were used without any further purification processes.

2.2. Methods

2.2.1. Pulping process

Wheat straw was subjected to a pulping process using 7% (o.d.m.) sodium hydroxide at 100 °C for 150 min as described by Espinosa et al. [21]. Unbleached pulp was bleached using 0.3 g of sodium chlorite per g of pulp in a 0.3% pulp suspension in water at 80 °C for 3 h. Once cooled, the pulp was filtered and washed with acetone and distilled water.

2.2.2. Isolation of nanocellulose

The nanocellulose samples were obtained using two different pretreatments. The mechanical pre-treatment consists of pulp refining in a PFI beater according to the ISO 5264-2:2002 for 20,000 rpm to achieve a drainage rate of 90 °SR. The TEMPO-mediated oxidation pretreatment was carried out as described by Besbes et al. [37]. A 5 mmol oxidation degree of TEMPO-mediated oxidation was performed adding the appropriate amount of 12% NaClO solution with continuous stirring at room temperature. The pH of the reaction was maintained at 10 by adding 0.5 M NaOH until no pH decrease was observed (≈ 2 h). Once finished, the reaction was stopped adding 100 mL of ethanol and the s were washed several times with distilled water. After the pretreatment, a 1 wt% fiber suspension was passed through a high-pressure homogeneizer (Panda GEA 2 K Niro) following the sequence: 4 passes at 300 bars, 3 passes at 600 bars and 3 passes at 900 bars [38]. Unbleached pulp was used to obtain LCNF from both pretreatments, however, bleached pulp was used only to obtain CNF through mechanical pre-treatment.

2.2.3. Nanocellulose characterization

The nanofibrillation yield was determined by centrifugation of a 0.1% nanocellulose suspension for 20 min at 10,000 rpm following the protocol described by Besbes et al. [37]. The optical transmittance of a 0.1% nanocellulose suspension was measured from 400 to 800 nm in a Lambda 25 UV-Spectrometer using distilled water as reference. The cationic demand was measured in a Particle Charge Detector (Mütek PCD 05) until reach a 0 mV value using the methodology described in the literature [39,40]. The cationic demand was calculated according to the equation proposed by Carrasco et al. [39]. The carboxyl content for the nanocellulose was determined by conductimetric titration, following the methodology described by Besbes et al. [37]. The cationic demand and carboxyl content values were used for a theoretical estimation of specific surface and diameter of nanocellulose, showing similar values than those obtained by TEM observation (±1 nm), as described in literature [39,40]. The values of intrinsic viscosity (η_s) for each sample were obtained following the ISO 5351:2010 standard. Five measures for each sample were obtained and the average and the standard deviation were calculated. The intrinsic viscosity value was used to calculate the degree of polymerization (DP) of the nanocellulose [41]. The degree of polymerization is related with the individual nanofiber length empirically, using the equation described by Shinoda et al. [42]:

$$Length\ (\mathrm{nm}) = 4.286 \cdot DP - 757$$

2.2.4. Preparation of PVA/nanocellulose biocomposite films

The solution of PVA (3 wt%) was prepared in distilled water and poured into a round bottom flask at 90 °C during 4 h with mechanical agitation. Nanocellulose was added in various concentrations 1, 3, 5 and 7% (w/w). The mixtures were further stirred for 4 h at room temperature and the suspensions were cast in polypropylene petri dishes (ø = 9 cm) and placed at room temperature until evaporation. The total dry weight of the mixture was 0.35 g per film.

2.3. Characterization techniques

2.3.1. Structural analysis

The surface and cross-section morphology of the biocomposite films was assessed with Scanning Electron Microscopy (SEM). The microscope was a Hitachi SU3500 Scanning Electron Microscope. The acceleration voltage and working distance was 5 kV and 6 mm, respectively.

The surface roughness was assessed with a Lehmann laser profilometer (Lehmann Mess-Systeme AG Baden-Dättwil, Germany). The topography images were 1 × 1 mm, with a resolution of 1 μm/pixel. The surface topography images were processed with the SurfChar] plugin for ImageJ, as described by Chinga-Carrasco et al. [43].

2.3.2. Fourier transform infrared spectroscopy analysis (FTIR)

FTIR Spectra of the films were recorded on FTIR-ATR Perkin-Elmer Spectrum Two. The resulting FTIR spectra were analysed to compare the effects of nanocellulose incorporated into PVA. The spectrum was analysed with a resolution of 4 cm^{-1} in the range of 450–4000 cm^{-1}. A total of 40 scans were collected for each sample.

2.3.3. X-ray diffraction analysis (XRD)

X-ray diffraction analysis was performed using a Bruker D8 Discover with a monochromatic source CuKα1 over an angular range of 5–50° at a scan speed of 1.56°/min. The crystallinity index of nanocellulose was calculated using the following equation [44]:

$$Crystallinity\ index\ (\%) = [(I_{200} - I_{am})/I_{200}] \cdot 100$$

where, I_{200} is the maximum intensity of the crystalline fraction at 2Θ between 22° and 24°, and I_{am} is the value of the intensity of the amorphous region, associated to the valley between the peaks at 22° and 15°.

2.3.4. Optical properties

The light transmittance of the film was determined using a Lambda 25 UV-Spectrometer from 400 to 800 nm. The percent transmittance at 660 nm (T_{660}) and 280 nm (T_{280}) was used to evaluate the light transmittance and UV barrier properties of the film, respectively [45].

2.3.5. Antioxidant activity

The antioxidant activity of the film was determined by the ABTS assay. A 7 mM ABTS and 2.45 mM potassium persulphate was prepared and kept in dark overnight before using. The absorbance of the solution at 734 nm was adjusted to 0.70 ± 0.02 diluting with ethanol. The analysis of the samples was carried out by mixing 4 mL of the radical solution where 1 cm^2 of the film was added and the absorbance was measured at 734 nm against ethanol. The absorbance of all the samples, including blank, were measured after 6 min and the antioxidant power (reduction of ABTS radical) was determined using the following equation [46]:

$$AOP = \%reduction\ of\ ABTS_{734} = \frac{A_{734,ABTS6'} - A_{734,film6'}}{A_{734,ABTS0'}} \cdot 100$$

where $A_{734,ABTS6'}$ is the absorbance at 734 nm of the radical solution after 6 min, $A_{734,film6'}$, the absorbance at 734 nm of the sample after 6 min and $A_{734,ABTS0'}$, the absorbance at 734 nm of the radical solution before the 6 min. ABTS scavenging activity was expressed in terms of antioxidant power per unit μg weight of the film (relative AOP).

2.3.6. Barrier properties

The water vapor transmission rate (WVTR) of the films was determined according to ASTSM E96/E96M-10 standard. The films were mechanically sealed with aluminium adhesive tape on plastic containers containing $CaCl_2$ as desiccant material. Then, containers were placed in a controlled chamber at 25 °C and a 50% relative humidity and weighted at different times interval to determine the mass gain. The mass gain was used to calculate the WVTR using the following equation [47]:

$$WVTR = \frac{\Delta W/t}{A}$$

where ΔW is the mass gain of the container at time t; and A is the effective area of exposed film ($78.54 \cdot 10^{-4}\ m^2$).

The thickness (I) and the difference in vapor partial pressure at both sides of the films was used to calculate the WVP.

$$WVP = \frac{WVTR \cdot I}{P_{sat} \cdot (RH_{out} - RH_{in})}$$

where RH_{out} and RH_{in} are the relative humidity's of the external (50%) and internal sides (0%) of the film, and the P_{sat} is the saturated vapor pressure at 25 °C (1583.7 Pa).

The Oxygen Transmission Rate (OTR) of film was measured using Mocon OX-TRAN® 1/50 test system (Mocon, Minneapolis, MN, USA) at 50% RH and 23 °C. At least three samples per film were measured and average value was calculated.

2.3.7. Mechanical properties

The Tensile Strength, Elongation at Break and Young Modulus of the films with different proportions of nanocellulose was determined using a LF Plus Lloyd Instrument testing machine provided with 1 kN load cell in accordance with the test method ASTM D638. Test specimens with 65 mm of length, 15 mm of width and 0.03 mm of thickness was prepared and conditioned for 48 h at 25 °C and 50% RH before testing. Ten specimens of each samples were tested.

3. Results and discussion

3.1. Nanocellulose characterization

Wheat straw was subjected to a soda pulping process. The cellulosic pulp contained 59.2% of α-cellulose content, 9.0% of lignin, 23.3% of hemicellulose, 1.5% of ashes, and 5.2% of extractables [21]. The cellulose pulp was bleached using sodium chlorite to remove lignin and maintain the content of hemicellulose and α-cellulose in the fiber. Hence, lignin-free cellulose nanofibers (CNF) were obtained by subsequently using mechanical pre-treatment followed by high pressure homogenizer (CNF-Mec). The unbleached pulp was used to obtain lignocellulose nanofibers (LCNF) using two different pre-treatments, mechanical (LCNF-Mec) and TEMPO-mediated oxidation (LCNF-TO). These samples were used to assess the effect of lignin on the reinforcement potential of nanocellulose in PVA biocomposite films. Additionally, the effect that

Table 1
Characterization of the different nanocelluloses.

Sample	Yield (%)	T_{800} (%)	CD (μeq·g/g)	CC (μeq·g/g)	σ_{spec} (m^2/g)	Diameter (nm)	Degree of polymerization (DP)	Length[a] (nm)
LCNF-Mec	55.6 ±5.26	55	441.06 ±7.50	64.41 ±2.36	183.42	13	1328	4939
LCNF-TO	>95	<90	1116 ±45.16	362.4 ±4.94	367.01	7	502	1395
CNF-Mec	27.09 ±5.47	34	328.69 ±37.19	51.24 ±1.19	125.50	20	1330	4943

[a] Length obtained from DP values using equation described by Shinoda et al. *Length (nm) = 4.286·DP-757.*

Table 2
Optical and UV-light blocking properties of the films.

Sample	Light transmittance (%)	T_{660} (%)	T_{280} (%)	T_{280}/T_{660}	UV absorption (%)
PVA	0	89.09	80.20	0.9020	9.98
1% LCNF-Mec	74.34	78.90	54.42	0.7843	21.57
3% LCNF-Mec	67.65	60.59	42.43	0.7022	29.78
5% LCNF-Mec	63.12	52.84	30.26	0.5723	42.77
7% LCNF-Mec	56.07	45.69	20.86	0.4564	54.36
1% LCNF-TO	90.39	76.35	59.22	0.7754	22.46
3% LCNF-TO	76.14	64.13	44.14	0.6860	31.40
5% LCNF-TO	67.21	60.65	34.55	0.6043	39.57
7% LCNF-TO	60.12	58.79	31.10	0.5291	47.09
1% CNF-Mec	87.15	85.49	7.83	0.8839	11.61
3% CNF-Mec	66.21	77.20	67.84	0.8671	13.29
5% CNF-Mec	59.21	49.38	35.43	0.7537	24.63
7% CNF-Mec	53.06	39.31	26.37	0.6912	30.88

TEMPO-mediated oxidation on the production of LCNF was assessed. Once the different nanocelluloses were prepared, they were characterized in terms of nanofibrillation yield, optical transmittance at 800 nm, cationic demand and carboxyl content (Table 1).

It is observed that the LCNF obtained by TEMPO-mediated oxidation (LCNF-TO) presents the highest nanofibrillation yield in comparison with the nanocellulose obtained by mechanical pre-treatment. These results were expected by the studies reported in bibliography by several authors [48–50]. The formation of negatively charged carboxyl groups in the C6 of the cellulose chains during the TEMPO-mediated oxidation leads to repulsive forces between nanofibers, promoting thus water uptake, fiber swelling, and higher yields (over 95%). The lower yield of samples obtained by mechanical pre-treatment denotes that these samples are composed by fibers with nanometric sizes and fibers with higher diameters, microfibers. In addition, this is reflected in the optical transmittance of the nanocellulose dispersion, where the samples with

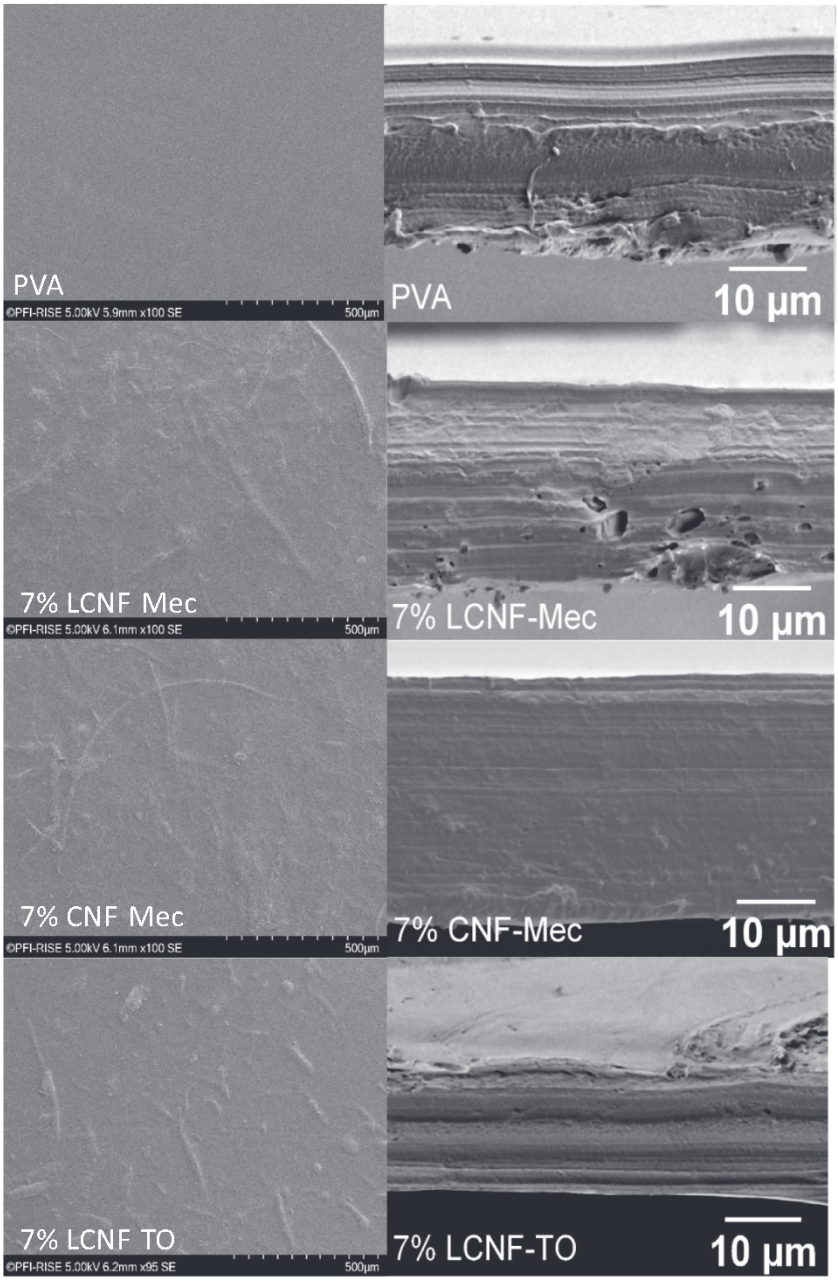

Fig. 1. SEM micrographs of biocomposite films: left) Surface, right) Cross-section.

higher nanofibrillation yields a higher transmittance due to the less light scattering caused by optically inactive nanofibers.

In relation to the effect of the chemical composition in the obtaining of nanocellulose, it was observed that lignin favours fibrillation. Hence, this resulted in higher nanofibrillation yield compared to lignin-free samples. The charge density and mechanoradical effects due to the lignin presence in the fiber affect the fibrillation, producing nanocellulose with smaller diameter, smaller pore structure, higher surface area and increased interaction with water [26]. The cationic demand of nanocellulose is affected by two parameters: i) carboxyl content, and ii) the specific surface of the nanofibers. The carboxyl content of TEMPO-oxidized nanocellulose presents higher carboxyl content due to the selective oxidation of C6 primary alcohol groups into carboxylic acid groups, in comparison with the samples subjected to mechanical pre-treatment. The surface charge of the LCNF-TO surface allows a greater electrostatic repulsion of the fibers, obtaining nanocellulose with a smaller diameter, and therefore a larger specific surface, thus presenting high values of cationic demand.

About the lignin content, there is a slight decrease in the diameter of the nanocellulose obtained from unbleached pulp (LCNF-Mec) in line with the yield values obtained, in comparison with those obtained from bleached pulp (CNF-Mec). In the case of TEMPO-oxidized nanocellulose, a strong depolymerization was evidenced by the reduction in the length in comparison with the other samples (Table 1). It is produced by the excessive oxidation of the amorphous regions of cellulose during the TEMPO-mediated oxidation, producing molecular fragments split from these regions that degrade completely into gluconic acid or small fragment dissolved by cellulose depolymerization and β-elimination [51].

3.2. Characterization of PVA/Nanocellulose films

3.2.1. Optical properties

The optical properties of the neat PVA, and PVA with varying proportions of different nanocellulose were determined by measuring the transmittance in the range of 200–800 nm (Fig. S1). The translucency of the film, the percent transmittance at 280 and 660 nm and the UV-light blocking for the different films were analysed (Table 2). The optical transmittance of the films is largely dependent on the dispersion of the nanocellulose in the PVA matrix. As the light transmittance values show, the film become relatively opaque with increasing nanocellulose content, decreasing from 95% light transmittance for pure PVA to 56% (LCNF-Mec), 60% (LCNF-TO) and 53% (CNF-Mec), when the nanocellulose content is maximum. The TEMPO-oxidized nanocellulose reduces to a lesser extent the light transmittance of PVA biocomposite films in relation to the higher content of nanofibrillated material (higher nanofibrillation yield) compared to the rest, revealing a better dispersion in the matrix. Fig. S2 shows how the film becomes opaquer when they contain nanocellulose, acquiring a slight brown colour in those reinforced with lignin-containing nanocellulose, especially for LCNF-Mec.

Neat PVA films showed high translucency, about 95%, but exhibited low UV light absorption capacity, blocking only the 10% of the UV-B range. As well as all the nanocelluloses cause a decrease in the transparency of the films, it increased significantly the capacity of UV absorption. With respect to the chemical composition of nanocellulose, it is observed how the nanocellulose with lignin content causes a greater increase in the UV absorption, which was mainly due to the phenolic groups and conjugated carboxyl groups present in lignin. It shows how the samples with lignin achieve UV blockage values of 54% and 47% for those obtained by mechanical pre-treatment and TEMPO-mediated oxidation, respectively. However, nanocellulose with no lignin content shows a significantly lower value, reaching only 30% absorption to UV light.

3.2.2. Structural characterization

SEM analysis of the different films was performed to study the microstructure and dispersion of nanocellulose into PVA biocomposite (Fig. 1). The micrographs showed that pure PVA film has a smoother surface compared to the biocomposites containing nanocellulose. As the nanocellulose content increase, the surface roughness of the biocomposites also increases as a result of the agglomeration of the nanofibers. The cross-section of pure PVA and nanocellulose reinforced PVA biocomposite films was also analysed. This examination is important to determine the distribution and interaction of nanocellulose into the PVA matrix. The cross-section observation clearly reveals that nanocellulose was randomly dispersed without precipitation into the PVA suspension during the casting process, showing a uniform cross-section without layer differentiation. In order to quantify the effect of nanocellulose on film roughness, a laser profilometry analysis was carried out (Fig. S3). Fig. 2 shows the obtained values of film surface roughness. As previously observed, the increase in nanocellulose content increases the roughness of the films. In addition, there are differences in the roughness contribution of the different nanocelluloses. The LCNF-Mec are the ones that produce the greatest increase in roughness due to the extra contribution generated by the residual lignin content in fiber [52]. LCNF-TO produce less effect on the roughness of films due to their reduced diameter, as well as their higher nanofibrillation in comparison with nanofibers obtained by mechanical pre-treatment. However, the elimination of lignin allows CNF-Mec to present values like those obtained by LCNF-TO despite the lower nanofibrillation.

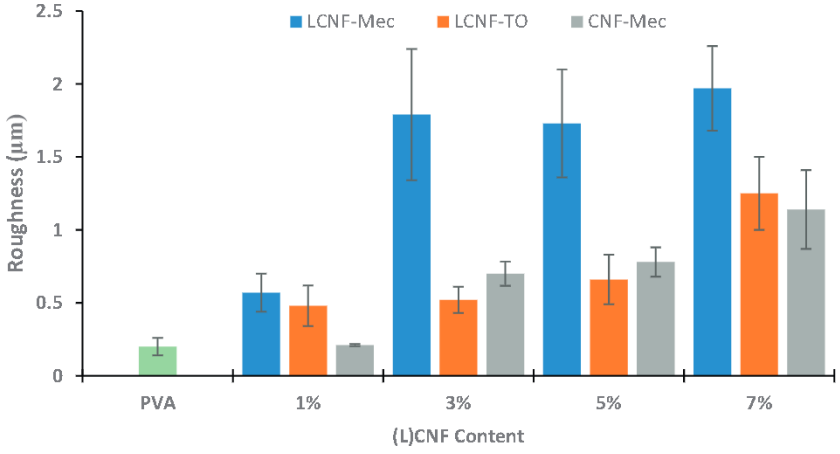

Fig. 2. Surface roughness quantification of biocomposite films.

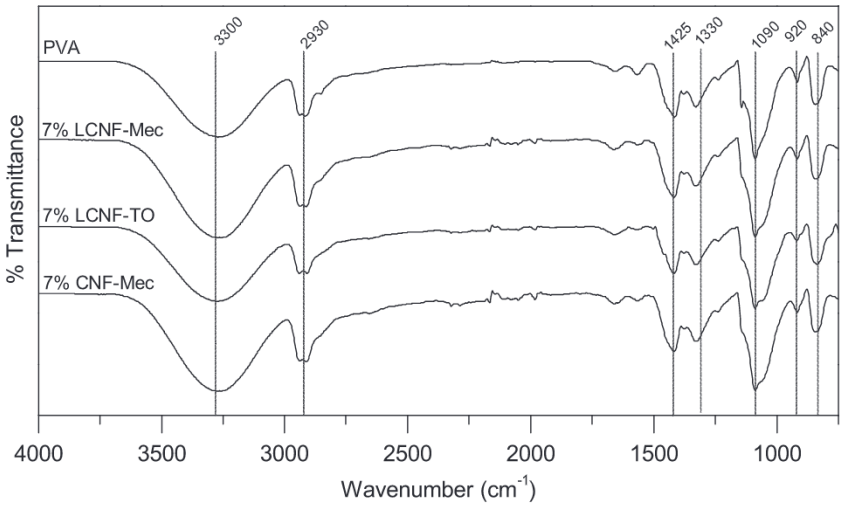

Fig. 3. ATR-FTIR spectra of neat PVA and PVA/nanocellulose biocomposite films.

3.2.3. FTIR and XRD analysis

The FTIR spectra of pure PVA and PVA/nanocellulose films (7%) were obtained to analyze the changes in chemical structure as a result of the introduction of LCNF and CNF (Fig. 3). All the spectra showed peaks at 3300 cm ^{1} indicating the stretching vibrations of O—H groups owing to the strong intermolecular and intramolecular bonds. The peak at 2930 cm ^{1} is associated to the stretching vibration of C—H from methyl or methylene groups, and in the range of 1500–800 cm ^{1} several peaks were identified, at 1425 cm ^{1} assigned to symmetric bending mode of CH_2 groups, at 1330 and 1043 cm ^{1} associated with the deformation of C—O groups, at 920 cm ^{1} assigned to syndiotactic structure of CH_2 groups and at 840 cm ^{1} assigned to stretching vibrations of C—C groups [17]. The regular PVA peaks were observed in the PVA/nanocellulose film spectra, indicating that the addition of the different nanocellulose had no significant influence in the molecular structure of PVA. The chemical composition of the different nanocelluloses is typical of lignocellulosic materials (Fig. S4) but show slight differences such as the peak increase at 1605 cm ^{1} in the LCNF-TO due to the increase of the carboxyl groups by the action of the TEMPO oxidation and the decrease and disappearance of the peak at 1510 cm ^{1} for LCNF-TO and CNF-Mec associated with the C=C bonding of the aromatic rings of the lignin structure, confirming a partial oxidation of the lignin in the TEMPO oxidation and the elimination of the lignin in the bleaching stage.

The crystalline structure of the films was tested by the X-ray diffraction (XRD) analysis. The X-ray diffraction patterns of neat PLA and PLA/Nanocellulose films are presented in Fig. 4. The diffraction peak of neat PVA is showed at $2\theta = 19.8°$ is associated to the hydrogen bonding between the hydroxyl groups of the PVA chains [53]. All the nanocellulose samples present the typical crystalline structure of cellulose I showing peaks at $\theta = 15.8°$ and $\theta = 22.4°$, corresponding to the (110) and (200) planes (Fig. S5). The crystallinity index of the different nanocelluloses was obtained using the methodology described by Segal et al., [44] obtaining values of 53.48%, 44.44% and 58.34% for LCNF-Mec, LCNF-TO and CNF-Mec, respectively. The crystallinity of LCNF-TO is decreased due to the degradation of crystalline cellulose during the TEMPO-mediated oxidation and the CNF-Mec presents a higher value than LCNF-Mec due to the removal of lignin as amorphous component. The diffraction patterns of the assessed PVA/nanocellulose are the results of the superposition of both materials, showing a slight both sides-shift asymmetry of the PVA peak due to adjacent crystalline signals.

3.2.4. Mechanical properties

The Fig. 5 shows the mechanical properties (tensile strength, elongation and Young's modulus) of the PVA films and its evolution with the addition of the different nanocelluloses. The thickness and density values of the PVA/nanocellulose biocomposites films are shown in Table S1. The thickness of the neat PVA film was 30 ± 3 μm, which was not modified significantly after the addition of nanocellulose. Regarding density, a slight increase is observed as the film contains more nanocellulose, due to the difference in density between nanocellulose (1.58 g/cm^3) and PVA (1.35–1.45 g/cm^3) [22]. For tensile strength a significant increase is observed with the incorporation of nanocellulose into the matrix, as well as a progressive increase when the content of nanocellulose is higher. A similar behaviour is observed when analysing the elastic modulus (Young's modulus) of the films, where a similar trend is followed with the increase of nanocellulose content. The increase of mechanical properties of PVA films with the addition of nanocellulose is attributed to the i) inherent chain stiffness and rigidity of nanocellulose (due to the extensive intermolecular and intramolecular hydrogen bonding with itself); ii) the homogeneous distribution of the nanocellulose in the PVA matrix, and; iii) the high compatibility between the nanocellulose and PVA, resulting in strong interaction through hydrogen bonding. Although a similar trend is observed when adding different nanocelluloses, not all of them produce the same reinforcing effect on the PVA matrix. Regarding to the tensile strength the neat PVA film shows a value of 43.60 MPa, increasing these values with the addition of nanocellulose to 72.76 MPa for LCNF-Mec, 63.96 MPa for LCNF-TO and 58.86 for CNF-Mec. On the other hand, the elastic modulus is

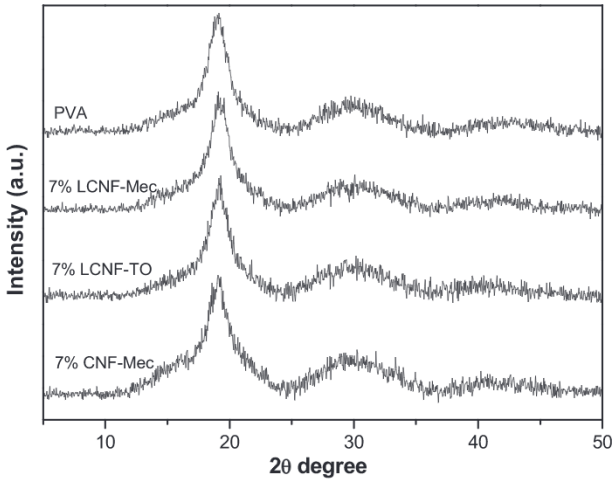

Fig. 4. X-ray diffractograms of the pure PVA and PVA/nanocellulose films.

increased in the same way by increasing the value of 2100 MPa exhibited by the pure PVA film to 5045 MPa, 4294 MPa and 4307 MPa for LCNF-Mec, LCNF-TO and CNF-Mec, respectively.

The differences in the reinforcement effect of the nanocellulose can be explained by the aspect ratio variations that they present. The aspect ratio values for the different nanocelluloses are 379 for LCNF-Mec, 205 for LCNF-TO and 248 for CNF-Mec. The length in several micrometers and the nanometric diameter of the nanocellulose results in a high surface area that allows these nanomaterials to reinforce a wide variety of polymers even at low loadings, improving the stiffness, strength, toughness, thermal stability and barrier properties compared to the neat polymer matrix [54].

Residual lignin content may also influence the reinforcing effect of nanocellulose in polymer matrices. Previous studies [26,55] reported that nanocellulose with residual lignin content yields higher specific surface area and lignin-related radicals which lead to crosslinking reaction, contributing to densification of the CNF structure. In addition, during the high pressure homogenization treatment, the lignin nanoparticles are detached from the nanocellulose and, due to their sticky nature, they adhere to the cellulosic nanofibers in the diluted

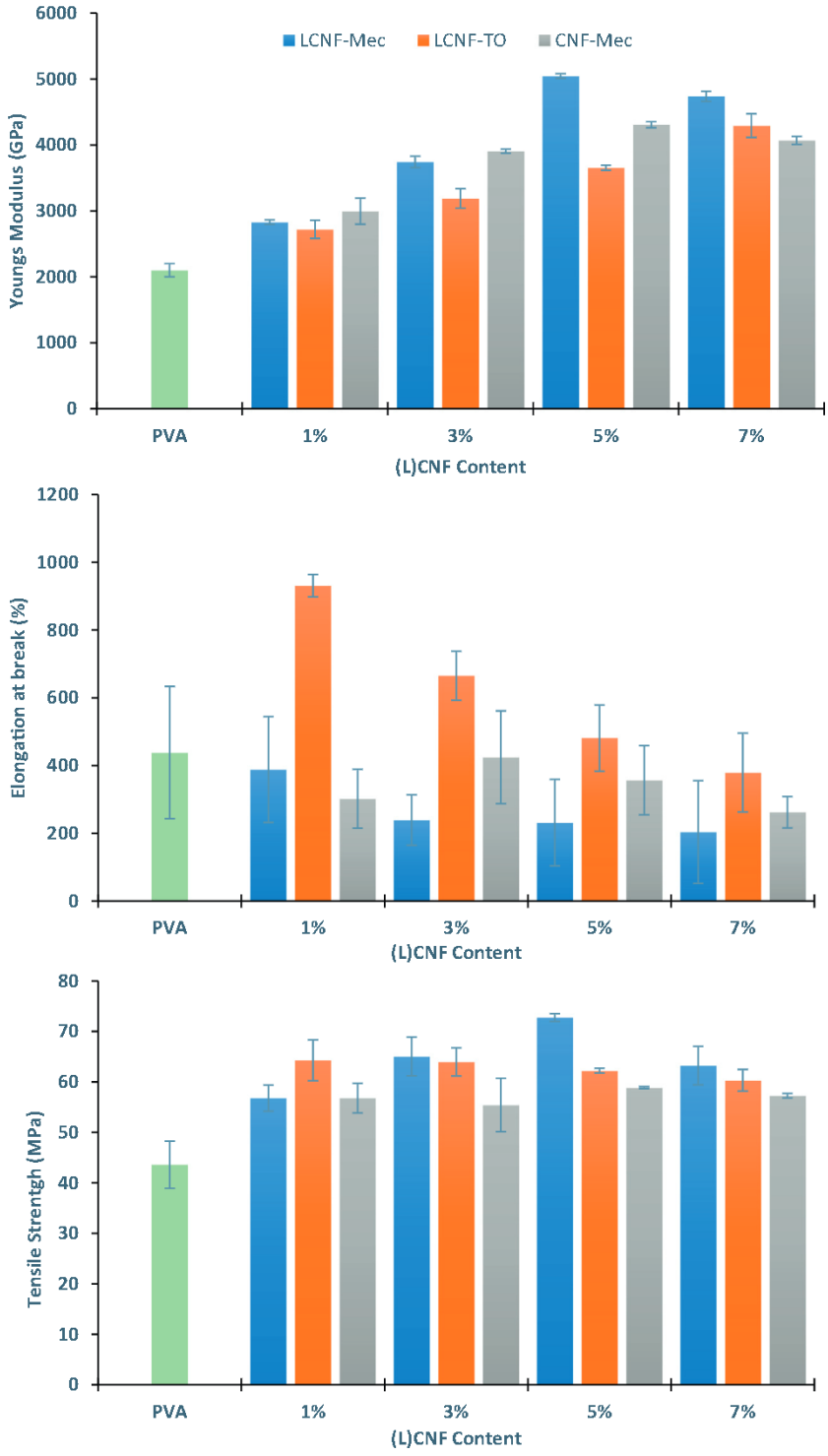

Fig. 5. Mechanical properties (Tensile Strength, Young's Modulus, Elongation at break) of PVA/nanocellulose biocomposite films.

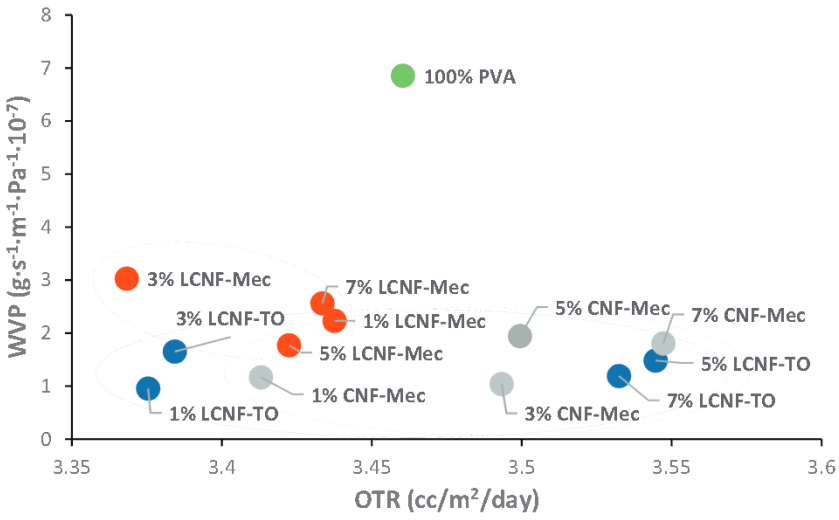

Fig. 6. Barrier properties of PVA/nanocellulose biocomposite films.

LCNF suspension. During the film formation, the amorphous nature of the lignin allows it to act as a filler in the gaps of the structure, acting as adhesive between fibers and produce a plasticizing effect [25]. In this work it is also observed that nanocellulose with a residual lignin content generally provide a greater reinforcement effect on the PVA matrix, even LCNF-TO with a lower aspect ratio. A decreasing trend is observed in the mechanical properties of the films when the nanocellulose load is higher than 5%. The decreasing trend with increasing contents of nanocellulose can be explained by the clustering of the nanocellulose in the PVA matrix, which act as weak spots initiating the ultimate failure of the composite [56]. Exceptionally, the elongation is significantly increased with LCNF-TO due to the water up taking of oxidized fiber that allows the break of intermolecular bonds and increase the polymer chain mobility [56]. In contrast to the rest of mechanical properties, the elongation at break decreases due to the increase in nanocellulose content. It can be associated to the intra or intermolecular hydrogen bonding of nanocellulose with PVA increasing the stiffness of the material and reducing the elasticity [57].

3.2.5. Barrier properties

Barrier properties of the biocomposite films were evaluated in terms of water vapor (WVP) and oxygen (OP) permeability (Fig. 6). The WVP decreased significantly as the nanocellulose content increased up to 1% and remained constant thereafter irrespective of the nanocellulose used. In comparison, OTR does not decrease significantly when nanocellulose content increases. In this case, the optimal value to obtain the lowest oxygen permeability value is 3% nanocellulose content, increasing the permeability again at 5 and 7%. The diffusion of gases in films occurs mainly in three steps: i) the absorption of gas molecule in the film surface; ii) the diffusion of the gas molecule through the film; and iii) the desorption of the gas molecule from the film to the other side [58]. The addition of nanocellulose acts in several steps of the diffusion process. Firstly, nanocellulose, despite its hydrophilic nature, decreases the hydrophilicity of the PVA matrix, thus decreasing the absorption of water vapor. Moreover, the presence of nanocellulose produces higher entanglements in the film matrix leading to a high density and a tortuous diffusion path for the gas molecules [59]. With respect to oxygen, nanocellulose samples with lignin produce a greater decrease in permeability due to its overall contributions in compacting the film structure making it less porous and therefore less permeable.

3.2.6. Antioxidant activity

The antioxidant power (AOP) of the films was measured using ABTS assay. The results of the antioxidant activity expressed per gram of film (Relative AOP) are presented in Fig. 7. The antioxidant measurement by this method is based on the amount of radical (2,2′-azino-di-[3-

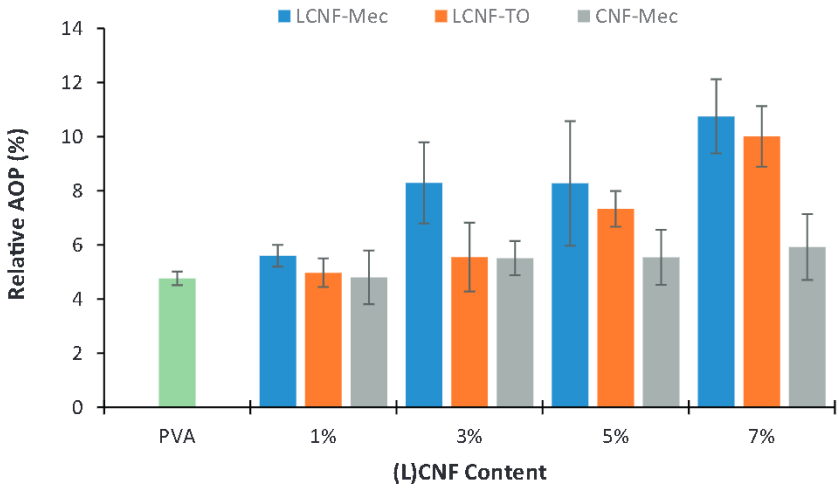

Fig. 7. Relative antioxidant power (AOP) of PVA/nanocellulose biocomposite films.

ethylbenzthiazoline sulfonate) reduced by the antioxidant components of the films. An increasing trend in the antioxidant power of the films is observed as the nanocellulose content increases, except for the lignin-free nanocellulose. This fact indicates that the increase in antioxidant power derives from the residual lignin content in nanocellulose due to the aromatic structure of lignin which acts as antioxidant agent preventing or retarding oxidation processes induced by oxidizing species, such as free radicals [60]. The AOP of the films was increased from 4.76 ± 0.25% of neat PVA to 10.75 ± 1.37% and 10.01 ± 1.12% for LCNF-Mec and LCNF-TO, respectively. However, the addition of CNF-Mec presents only an AOP of 5.92 ± 1.22%. It is therefore concluded that the presence of lignin in nanocelluloses produces films with higher antioxidant capacity, and that TEMPO oxidation does not produce a significant oxidation of the chemical structure of lignin, maintaining AOP levels similar to those obtained using mechanical nanocellulose.

4. Conclusions

In the present study, we analysed the effect of nanocellulose as reinforcing agent in PVA biocomposites films. In addition, the effect of residual lignin content and the pre-treatment in nanocellulose production was also studied. PVA/nanocellulose biocomposites films were successfully produced using solution casting method. The UV-light blocking properties of the films was enhanced incorporating nanocellulose into PVA matrix, especially for lignin-containing nanocellulose (>50%). The mechanical properties of the films were significantly improved by the addition of nanocellulose, however, from loads higher than 5% there is a decrease in the trend due to a potential clustering of nanocellulose components. The TEMPO-mediated oxidation reduces the reinforcing effect of nanocellulose due to the degradation and shortening of the fibers. The barrier properties to water vapor and oxygen of the films was also improved by incorporating nanocellulose. The antioxidant capacity of the films was increased when using lignin-containing nanocellulose from 4.7% of pure PVA to >10%.

Acknowledgments

The authors are grateful to Spain's DGICyT, MICINN for funding this research within the framework of the Projects CTQ2016-78729-R and supported by the Spanish Ministry of Science and Education through the National Program FPU (Grant Number FPU14/02278), and also to the staff of the Central Service for Research Support (SCAI) at the University of Córdoba.

Appendix A. Supplementary data

Supplementary data to this article can be found online at https://doi.org/10.1016/j.ijbiomac.2019.08.262.

References

[1] V. Siracusa, P. Rocculi, S. Romani, M.D. Rosa, Biodegradable polymers for food packaging: a review, Trends Food Sci Tech 19 (2008) 634–643.
[2] M.M. Ibrahim, W.K. El-Zawawy, M.A. Nassar, Synthesis and characterization of polyvinyl alcohol/nanospherical cellulose particle films, Carbohyd Polym 79 (2010) 694–699.
[3] E. Chiellini, P. Cinelli, S.H. Imam, L. Mao, Composite films based on biorelated agro-industrial waste and poly(vinyl alcohol) preparation and mechanical properties characterization, Biomacromolecules 2 (2001) 1029–1037.
[4] K.Y. Lee, T. Tammelin, K. Schulfter, H. Kiiskinen, J. Samela, A. Bismarck, High performance cellulose nanocomposites: comparing the reinforcing ability of bacterial cellulose and nanofibrillated cellulose, ACS Appl Mater Inter 4 (2012) 4078–4086.
[5] A.G. El-Shamy, A.A. Maati, W. Attia, K.M. Abd El-Kader, Promising method for preparation the PVA/Ag nanocomposite and Ag nano-rods, J Alloy Compd 744 (2018) 701–711.
[6] A. Akhavan, F. Khoylou, E. Ataeivarjovi, Preparation and characterization of gamma irradiated starch/PVA/ZnO nanocomposite films, Radiat. Phys. Chem. 138 (2017) 49–53.
[7] V. Kaler, U. Pandel, R.K. Duchaniya, Development of TiO2/PVA nanocomposites for application in solar cells, Mater Today-Proc 5 (2018) 6279–6287.
[8] L.N. Ludueña, V.A. Alvarez, A. Vazquez, Processing and microstructure of PCL/clay nanocomposites, Mater. Sci. Eng. A 460–461 (2007) 121–129.
[9] M. Jonoobi, Y. Aitomäki, A.J. Mathew, K. Oksman, Thermoplastic polymer impregnation of cellulose nanofibre networks: morphology, mechanical and optical properties, Compos Part A-Appl S 58 (2014) 30–35.
[10] C. Chen, D. Li, K. Abe, H. Yano, Formation of high strength double-network gels from cellulose nanofiber/polyacrylamide via NaOH gelation treatment, Cellulose 25 (2018) 5089–5097.
[11] X. Xu, F. Liu, L. Jiang, J.Y. Zhu, D. Haagenson, P.D. Wiesenborn, Cellulose nanocrystals vs. cellulose nanofibrils: a comparative study on their microstructures and effects as polymer reinforcing agents, ACS Appl Mater Inter 58 (2013) 2999–3099.
[12] J.Ø. Torstensen, R.M.L. Helberg, L. Deng, Ø.W. Gregersen, K. Syverud, PVA/nanocellulose nanocomposite membranes for CO2 separation from flue gas, Int J Greenh Gas Con 81 (2019) 93–102.
[13] Z. Jahan, M.B.K. Niazi, M.B. Hägg, Ø.W. Gregersen, Decoupling the effect of membrane thickness and CNC concentration in PVA based nanocomposite membranes for CO2/CH4 separation, Sep. Purif. Technol. 204 (2018) 220–225.
[14] R. Pramanik, B. Ganivada, F. Ram, K. Shanmuganathan, A. Arockiarajan, Influence of nanocellulose on mechanics and morphology of polyvinyl alcohol xerogels, J Mech Behav Biomed 90 (2019) 275–283.
[15] S. Agate, M. Joyce, L. Lucia, L. Pal, Cellulose and nanocellulose-based flexible-hybrid printed electronics and conductive composites – a review, Carbohyd Polym 198 (2018) 249–260.
[16] I. Gan, W.S. Chow, Antimicrobial poly(lactic acid)/cellulose bionanocomposite for food packaging application: a review, Food Pack Shelf Life 17 (2018) 150–161.
[17] M.S. Sarwar, M.B.K. Niazi, Z. Jahan, T. Ahmad, A. Hussain, Preparation and characterization of PVA/nanocellulose/Ag nanocomposite films for antimicrobial food packaging, Carbohyd Polym 184 (2018) 453–464.
[18] S. Iwamoto, W. Kai, A. Isogai, T. Iwata, Elastic modulus of single cellulose microfibrils from tunicate measured by atomic force microscopy, Biomacromolecules 10 (2009) 2571–2576.
[19] T. Saito, T. Uematsu, S. Kimura, T. Enomae, A. Isogai, Self-aligned integration of native cellulose nanofibrils towards producing diverse bulk materials, Soft Matter 7 (2011) 8804–8809.
[20] T. Nishino, I. Matsuda, K. Hirao, All-cellulose composite, Macromolecules 37 (2004) 7683–7687.
[21] E. Espinosa, R. Sánchez, R. Otero, J. Domínguez-Robles, A. Rodríguez, A comparative study of the suitability of different cereal straws for lignocellulose nanofibers isolation, Int. J. Biol. Macromol. 103 (2017) 990–999.
[22] J. Velásquez-Cock, C. Castro, P. Gañán, M. Osorio, J.L. Putaux, A. Serpa, R. Zuluaga, Influence of the maturation time on the physico-chemical properties of nanocellulose and associated constituents isolated from pseudostems of banana plant c.v. Valery, Ind. Crop. Prod. 83 (2016) 551–560.
[23] J.P.S. Morais, M.D.F. Rosa, M. de Souza Filho, L.D. Nascimento, D.M. do Nascimento, A.R. Cassales, Extraction and characterization of nanocellulose structures from raw cotton linter, Carbohyd Polym 91 (2013) 229–235.
[24] Ú. Fillat, B. Wicklein, R. Martín-Sampedro, D. Ibarra, E. Ruiz-Hitzky, C. Valencia, A. Sarrión, E. Castro, M.E. Eugenio, Assessing cellulose nanofiber production from olive tree pruning residue, Carbohyd Polym 179 (2018) 252–261.
[25] G. Chinga-Carrasco, N. Kuznetsova, M. Garaeva, I. Leirset, G. Galiullina, A. Kostochko, K. Syverud, Bleached and unbleached MFC nanobarriers: properties and hydrophobisation with hexamethyldisilazane, J. Nanopart. Res. 14 (2012) 1–10.
[26] A. Ferrer, E. Quintana, I. Filpponen, I. Solala, T. Vidal, A. Rodríguez, J. Laine, O.J. Rojas, Effect of residual lignin and heteropolysaccharides in nanofibrillar cellulose and nanopaper from wood fibers, Cellulose 19 (2012) 2179–2193.
[27] K. Abe, F. Nakatsubo, H. Yano, High-strength nanocomposite based on fibrillated chemi-thermomechanical pulp, Compos. Sci. Technol. 69 (2009) 2434–2437.
[28] E. Rojo, M.S. Peresin, W.W. Sampson, I.C. Hoeger, J. Vartiainen, J. Laine, O.J. Rojas, Comprehensive elucidation of the effect of residual lignin on the physical, barrier, mechanical and surface properties of nanocellulose films, Green Chem. 17 (2015) 1853–1866.
[29] W. Gindl-Altmutter, M. Obersriebnig, S. Veige, F. Liebner, Compatibility between cellulose and hydrophobic polymer provided by microfibrillated lignocellulose, ChemSusChem 8 (2015) 87–91.
[30] K.L. Spence, R.A. Venditti, Y. Habibi, O.J. Rojas, J.J. Pawlak, The effect of chemical composition on microfibrillar cellulose films from wood pulps: mechanical processing and physical properties, Bioresour. Technol. 101 (2010) 5961–5968.
[31] K.L. Spence, R.A. Venditti, O.J. Rojas, Y. Habibi, J.J. Pawlak, A comparative study of energy consumption and physical properties of microfibrillated cellulose produced by different processing methods, Cellulose 18 (2011) 1097–1111.
[32] M. Pishnamazi, H.Y. Ismail, S. Shirazian, J. Iqbal, G.M. Walker, M.N. Collins, Application of lignin in controlled release: development of predictive model based on artificial neural network for API release, Cellulose 26 (2019) 6165–6178.
[33] M. Pishnamazi, J. Iqbal, S. Shizarian, G.M. Walker, M.N. Collins, Effect of lignin on the release rate of acetylsalicylic acid tablets, Int. J. Biol. Macromol. 124 (2019) 354–359.
[34] N. Dalton, R.P. Lynch, M.N. Collins, M. Culebras, Thermoelectric properties of electrospun carbon nanofibres derived from lignin, Int. J. Biol. Macromol. 121 (2019) 472–479.
[35] M. Culebras, M.J. Sanchis, A. Beaucamp, M. Carsi, B.K. Kandola, A.R. Horrocks, G. Panzetti, C. Birkinshaw, M.N. Collins, Understanding the thermal and dielectric response of organosolv and modified Kraft lignin as a carbon fibre precursor, Green Chem. 20 (2018) 4461–4472.
[36] M. Culebras, H. Geaney, A. Beaucamp, P. Upadhyaya, E. Dalton, K.M. Ryan, M.N. Collins, Bio-derived carbon nanofibers from lignin as high performance Li-on anode materials, ChemSusChem (2019)https://doi.org/10.1002/cssc.201901562.
[37] I. Besbes, S. Alila, S. Boufi, Nanofibrillated cellulose from TEMPO-oxidized eucalyptus fibres: effect of the carboxyl content, Carbohyd Polym 84 (2011) 975–983.

[38] E. Espinosa, J. Dominguez-Robles, R. Sanchez, Q. Tarres, A. Rodriguez, The effect of pre-treatment on the production of lignocellulosic nanofibers and their application as a reinforcing agent in paper, Cellulose 24 (2017) 2605–2618.
[39] F. Carrasco, P. Mutje, M.A. Pelach, Control of retention in paper-making by colloid titration and zeta potential techniques, Wood Sci. Technol. 32 (1998) 145–155.
[40] E. Espinosa, Q. Tarres, M. Delgado-Aguilar, I. Gonzalez, P. Mutje, A. Rodriguez, Suitability of wheat straw semichemical pulp for the fabrication of lignocellulosic nanofibres and their application to papermaking slurries, Cellulose 23 (2016) 837–852.
[41] M. Marx-Figini, The acid-catalyzed degradation of cellulose linters in distinct ranges of degree of polymerization, J. Appl. Polym. Sci. 33 (1987) 2097–2105.
[42] R. Shinoda, T. Saito, Y. Okita, A. Isogai, Relationship between length and degree of polymerization of TEMPO-oxidized cellulose nanofibrils, Biomacromolecules 13 (2012) 842–849.
[43] G. Chinga-Carrasco, N. Averianova, O. Kondalenko, M. Garaeva, V. Petrov, B. Leinsvang, T. Karlsen, The effect of residual fibres on the micro-topography of cellulose nanopaper, Micron 56 (2014) 80–84.
[44] L. Segal, J.J. Creely, A.E. Martin, C.M. Conrad, An empirical method for estimating the degree of crystallinity of native cellulose using X-ray diffractometer, Text. Res. J. 29 (1959) 786–974.
[45] S. Shankar, X. Teng, G. Li, J.W. Rhim, Preparation, characterization, and antimicrobial activity of gelatin/ZnO nanocomposite films, Food Hydrocolloid 45 (2015) 264–271.
[46] A. García, M. González Alriols, G. Spigno, J. Labidi, Lignin as natural radical scavenger. Effect of the obtaining and purification processes on the antioxidant behaviour of lignin, Biochem. Eng. J. 67 (2012) 173–185.
[47] S.S. Karkhanis, N.M. Stark, R.C. Sabo, L.M. Matuana, Water vapor and oxygen barrier properties of extrusion-blown poly(lactic acid)/cellulose nanocrystals nanocomposite films, Compos Part A-Appl S 114 (2018) 204–211.
[48] M. Delgado-Aguilar, I. González Tovar, Q. Tarrés, M. Alcalá, M.A. Pèlach, P. Mutjé, Approaching a low-cost production of cellulose nanofibers for papermaking applications, BioResources 10 (2015) 5345–5355.
[49] I. González, S. Boufi, M.A. Pèlach, M. Alcalà, F. Vilaseca, P. Mutjé, Nanofibrillated cellulose as paper additive in eucalyptus pulps, BioResources 7 (2015) 5167–5180.
[50] T. Saito, S. Kimura, Y. Nishiyama, A. Isogai, Cellulose nanofibers prepared by TEMPO-mediated oxidation of native cellulose, Biomacromolecules 8 (2007) 2485–2491.
[51] X.K. Sang, C.R. Qin, Z.F. Tong, S. Kong, Z. Jia, G.C. Wan, X.L. Liu, Mechanism and kinetics studies of carboxyl group formation on the surface of cellulose fiber in a TEMPO-mediated system, Cellulose 24 (2017) 2415–2425.
[52] S. Shankar, J.P. Reddy, J.W. Rhim, Effect of lignin on water vapor barrier, mechanical, and structural properties of agar/lignin composite films, Int. J. Biol. Macromol. 81 (2015) 267–273.
[53] X. Sun, C. Lu, Y. Liu, W. Zhang, X. Zhang, Melt-processed poly(vinyl alcohol) composites filled with microcrystalline cellulose from waste cotton fabrics, Carbohyd Polym 101 (2014) 642–649.
[54] A. Dufresne, Nanocellulose: a new ageless bionanomaterial, Mater. Today 16 (2013) 220–227.
[55] S.S. Nair, N. Yan, Effect of high residual lignin on the thermal stability of nanofibrils and its enhanced mechanical performance in aqueous environments, Cellulose 22 (2015) 3137–3150.
[56] M.B.K. Niazi, Z. Jahan, S.S. Berg, Ø.W. Gregersen, Mechanical, thermal and swelling properties of phosphorylated nanocellulose fibrils/PVA nanocomposite membranes, Carbohyd Polym 177 (2017) 258–268.
[57] Y.C. Ching, A. Rahman, K.Y. Ching, N.L. Sukiman, H.C. Cheng, Preparation and characterization of polyvinyl alcohol-based composite reinforced with nanocellulose and nanosilica, BioResources 10 (2015) 3364–3377.
[58] S.S. Nair, J.Y. Zhu, Y. Deng, A.J. Ragauskas, High performance green barriers based on nanocellulose, Sustain Chem Process 2 (2014) 23–30.
[59] A. Ferrer, L. Pal, M. Hubbe, Nanocellulose in packaging: advances in barrier layer technologies, Ind. Crop. Prod. 95 (2017) 574–582.
[60] Q. Lu, W. Liu, L. Yang, Y. Zu, B. Zu, M. Zhu, Y. Zhang, X. Zhang, R. Zhang, Z. Sun, J. Huang, X. Zhang, W. Li, Investigation of the effects of different organosolv pulping methods on antioxidant capacity and extraction efficiency of lignin, Food Chem. 131 (2012) 313–317.